



# Multiphysics Design and Development of Heterogeneous Functional Materials for Renewable Energy Devices: The HeteroFoam Story

K. L. Reifsnider,<sup>a,z</sup> Wilson K. S. Chiu,<sup>b,\*</sup> Kyle S. Brinkman,<sup>c</sup> Yanhai Du,<sup>a</sup> Arata Nakajo,<sup>b</sup> Fazle Rabbi,<sup>a</sup> and Qianlong Liu<sup>a</sup>

<sup>a</sup>Department of Mechanical Engineering, University of South Carolina, Columbia, South Carolina 29209, USA

<sup>b</sup>Department of Mechanical Engineering, University of Connecticut, Storrs, Connecticut 06269, USA

<sup>c</sup>Savannah River National Laboratory, Aiken, South Carolina 29808, USA

The electrochemical science that makes many energy conversion and storage technologies work rests on our knowledge and understanding of heterogeneous materials and material systems. The function and functionality of those systems share many common features across a wide range of technologies including fuel cells, batteries, capacitors, and membranes. The science that controls that functionality for these complex material systems is typically summoned in fragments to design a specific device. The present paper discusses an attempt to create a codified multiphysics approach to that general subject, across multiple scales in space and time, for heterogeneous functional materials, or "HeteroFoam" as we call it. The scope of the paper will be necessarily limited to a general definition of the problem focused on a few specific examples of the progress made for directions that support technologies such as conversion of chemical energy to electricity, membranes for selective transport, and charge storage devices. The principal motivation for this approach is to establish the science that controls emergent properties in heterogeneous functional materials as a foundation for design of functional material systems with performance not bounded by constituent properties.

© 2013 The Electrochemical Society. [DOI: 10.1149/2.012306jes] All rights reserved.

Manuscript submitted December 31, 2012; revised manuscript received February 18, 2013. Published March 6, 2013. This was Paper 1761 presented at the Honolulu, Hawaii, Meeting of the Society, October 7–12, 2012.

## HeteroFoam as a Foundation Concept

The general concept of heterogeneous functional materials as a genre of material systems is presented in Fig. 1. As depicted, that general material has at least two solid phases, associated interfaces and phase boundaries, and a void phase which may function as a conduit for liquid or gas transport, i.e., a porous composite. Typically, energy, charge, and mass flow into and out of the system as a domain, so that at the global level one must consider the balance of mass, momentum, energy and charge. Since we wish to establish the fundamental science of such a functional material system, our ultimate goal is to use that science to design the details of the HeteroFoam, i.e., to specify the constituents, their morphology and geometry, and their interfaces (or interphases) to achieve a specified system function, such as converting a liquid fuel to electricity.

One of the greatest challenges and opportunities associated with the design of heterogeneous functional materials is to establish a rational and systematic approach to the specification of the extrinsic features of the material system. Some of the extrinsic features of HeteroFoam materials design are illustrated in Fig. 2. At the atomic level, defect chemistry has opened a new world of material design for conduction, transport, and dielectric character. For bulk materials, new atomic level analysis methods have provided a foundation for understanding and designing oxygen vacancy formation to enhance ionic conduction, delocalization of charge to enhance electronic conduction, and oxygen migration to enhance oxygen transport in solid oxide fuel cell (SOFC) cathodes, for example.<sup>1,2</sup> For functional surfaces and interfaces, quantum mechanics analysis has been combined with analysis of surface and interface processes to establish rate equations for electrochemical reactions.<sup>3</sup> These and other advances by our HeteroFoam Center team and their collaborators present essential elements of a foundation for rational constituent design of electrodes and mixed ionic and electronic conductors (MIECs) from first principles. This robust and complex story will be the subject of subsequent publications.

At the nano-level, recent discoveries indicate that there are many options for design, involving nano-phase distributions that, for example, enable the creation of new mechanisms for pseudo-capacitance in heterogeneous nano-materials involving combinations of redox and charge delocalization to achieve orders of magnitude increases in charge storage in such materials.<sup>4,5</sup> This, too, is a robust opportunity that we will discuss in detail in another venue.

The present paper addresses three examples of the design of heterogeneous functional materials that have foundations at the meso-level as a demonstration of the HeteroFoam concept and approach. First, we discuss the design of electrodes for intermediate temperature SOFCs with the general focus of accommodating the conversion of chemical energy from liquid fuels to electricity. Second, we discuss the design of MIEC solid state membranes for separation processes. And third, we address designing non-dilute heterogeneous dielectric mixtures for charge storage.

A final feature of the paper is the discussion of emerging properties in heterogeneous functional materials. This discussion has two elements. First, we briefly introduce the principles of collateral action vs. synergistic action of the constituents of a HeteroFoam. If the contribution of constituents to global properties is largely or exclusively determined by their individual properties, they simply act together, with the general laws of mixtures applicable to their collective collateral performance. If the constituents interact with each other, the global response may be very different from the properties of the individual constituents, and they are said to be emergent. In that case, the fundamental science of constituent interaction is essential to the design of the material system, and the system properties are not constrained by the individual properties of the constituents. HeteroFoam material systems are most often in the latter category. And because these systems (as shown in Fig. 1) usually involve an open domain (with, for example, fuel flowing in and out, etc.), they are often not in equilibrium, and not conservative. These characteristics give rise to a discussion of material state changes, the second fundamental element that drives emergent properties. We will close the present paper with a brief discussion of this basic characteristic of HeteroFoam design.

## Design of SOFC Electrodes

The concept of a HeteroFoam element can be introduced and motivated by the important application of conversion of liquid chemical fuels to electricity with Solid Oxide Fuel Cell (SOFC) devices. The following sections will then develop the concept of the HeteroFoam approach to SOFC electrode design.

An SOFC can be operated on multiple fuels, including liquid fuels such as ethanol and jet fuel utilizing catalyst reforming. The reformation process breaks H-C bonds into hydrogen rich gases or syngas which can be directly fed into SOFCs with technology currently available. The example provided here was a breadboard JP-8 SOFC system, which consisted of several sub-units: liquid fuel delivery, on-board miniature desulfurizer, vaporizer, catalyst reformer

\*Electrochemical Society Active Member.

<sup>z</sup>E-mail: Reifsnider@sc.edu

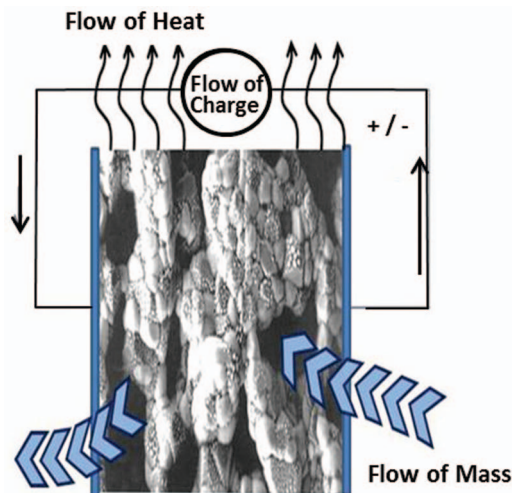
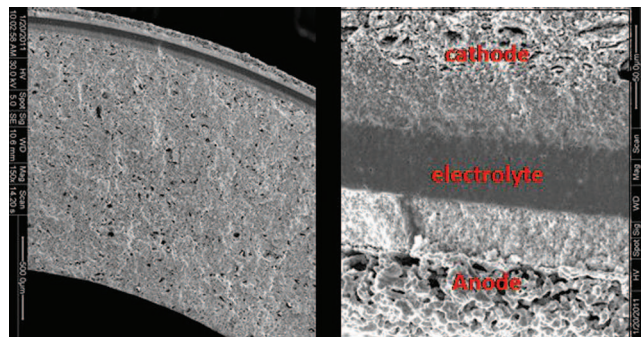


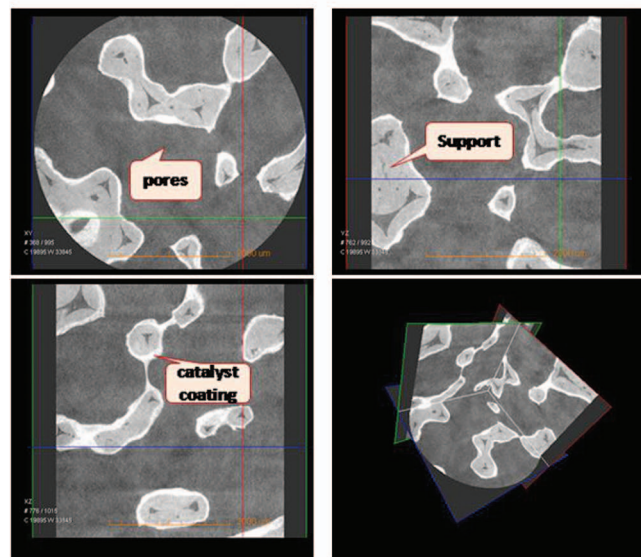
**Figure 1.** Illustration of the general concept of heterogeneous functional material, or HeteroFoaM ([www.HeteroFoaM.com](http://www.HeteroFoaM.com)).

and an SOFC stack. The design of SOFC electrodes (both anode and cathode) follows familiar general principles: maximizing the triple phase boundaries (TPB) and conductivities while maintaining stability. Anode-supported tubular SOFCs were used in this example. The porous microstructure of the nickel-based anode was essentially similar to that shown in Fig. 3. For portable applications, catalytic partial oxidation (CPOX) is a choice for JP-8 reforming due to its operational simplicity. The reforming catalyst can be uniformly coated onto porous ceramic supports, as shown in Fig. 3b (catalyst details are proprietary). We assembled a stack of tubular cells that generated over 100 watts of electric power and demonstrated reasonable stability and tolerance to sulfur over the tested 40 hours. Previous results have been published for SOFCs operating on other legacy fuels for over 1000 hours.<sup>6</sup>

These and other state-of-the-art results have been achieved on the basis of experience and Edisonian innovation, gained over a period of many years. They are the result of a collection of art and science which enables us to make a better fuel cell, but does not represent a



(a)



(b)

**Figure 3.** SEM micrographs of electrode morphologies (a), and morphology of JP-8 reforming catalyst samples, (b): catalyst coating (white), support (light gray) and pores (dark gray).

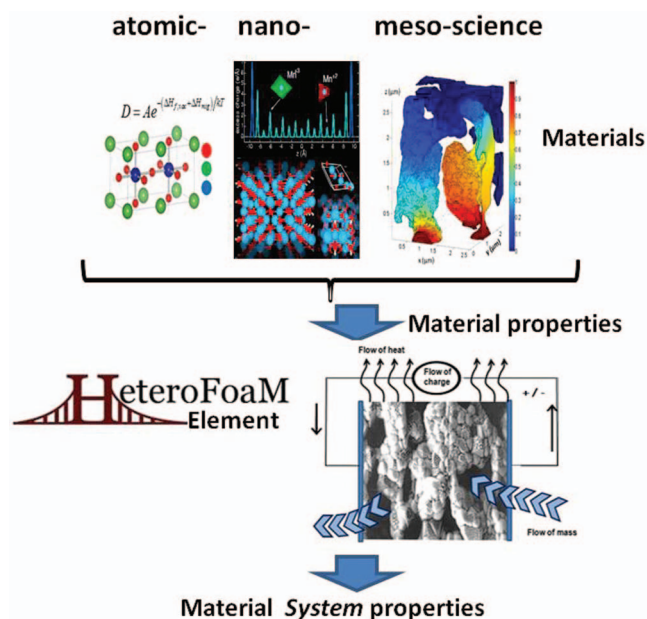


**Figure 2.** Illustration of the multiple space scales required to specify the design of a heterogeneous functional material system.

foundation for making fuel cells better. When lower temperature operation is needed, for example, to reduce cost, or when the inevitable variations in the chemical composition of liquid fuels are to be accommodated, or when regenerative or reversible SOFCs are to be designed, candidate materials are subjected to trials in myriad combinations. There is no comprehensive rational foundation for the knowledge based design of the functional material systems that must be created to make them work well. The present approach addresses that need.

*Challenges in SOFC electrode design.*— A solid oxide fuel cell electrode can be viewed as a system where ionic and electronic conduction takes place concurrently with gas-phase transport of reactants and products, respectively to and away from the electrochemically active sites. In the present work, efforts were made to reduce the polarization resistance by extending the active zone beyond the triple phase boundary (TPB) between the electrolyte and electrode. This effort included the development of porous electrode materials made of either a single-solid phase material exhibiting sufficient mixed ionic and electronic conduction, such as lanthanum strontium cobaltite ferrite (LSCF), or of heterogeneous materials, such as lanthanum strontium manganite and yttria-stabilized zirconia (LSM-YSZ). For both electrode types, button cell experiments have highlighted an exacerbated influence of the manufacturing processing parameters on the polarization resistance and material stability upon operation.<sup>7</sup>

Modeling approaches for electrode design have mostly focused on the case of heterogeneous electrode materials. They seek to provide guidance in the choice of the phase materials, the particle sizes of starting powders and volume fractions, including functional grading, to maximize the available triple-phase boundaries and transport within the structure. Tailoring of the coefficient of thermal expansion to ideally ensure shielding compressive stress in the thin layer is typically not included in the analysis. One approach is based on isothermal continuum composite electrode models coupled with percolation theory for the prediction of the effective conductivity and TPB length.<sup>8-12</sup> Another consists in applying discrete element methods to a domain of numerically sintered packed spheres, which provide a more rigorous treatment of grading and information into the effects of local geometry on the electrode properties.<sup>13</sup> Approaches are restricted to electrode fabrication routes that produce structures complying with the used idealized representation and possible combinations of materials where the elementary steps of the electrochemical reactions do not extend far beyond the TPB. Guidance is provided in terms of metrics that do not uniquely describe a structure. These are non-negligible limitations in the light of, among others, the crucial effect of the conditions during the reduction of the NiO-YSZ anode material before operation and continuous progresses of fabrication techniques toward a deterministic control of the produced structure. They partly explain why these modeling approaches have been used as electrode enhancement tools, rather than implemented as part of an optimization problem. As of today, their outcome still mainly consists in the explanation of experimentally observed trends, rather than driving design for expected performance.

The limitation of most models for electrode design to support specific fabrication routes is not the only reason why screening experiments largely remain the preferred choice for electrode development. The aforementioned view of an SOFC electrode is incomplete and cannot bridge the multiple relevant time and space scales depicted in Figure 2 with sufficient versatility, coherence and level of details. For design purposes, the electrodes should be treated as a heterogeneous system of functional materials following the HeteroFoAM concept and methodology defined and described. There, transport within the heterogeneous structure is not limited to that of ion, electron and gaseous species involved in heterogeneous energy conversion reactions. Thermodynamic potential gradients develop in the heterogeneous structure depending on the local conditions in an SOFC during constant load operation, following of the electrical load demand, or thermal cycling induced physico-chemical alterations of the phases. Processes involving the material constituents, such as surface segregation, demixing or gas-phase transport promoted by the formation of volatile species are indeed ascertained or suspected for most common SOFC materials.<sup>14,15</sup> Impurities within the starting materials and external contamination further promote detrimental alterations of the heterogeneous structure.<sup>16</sup> As a consequence, electrodes must be treated as a heterogeneous system of functional materials.

Screening experiments become excessively time-consuming and of questionable reliability for lifetime predictions under various conditions. The current knowledge is however not yet sufficient to treat electrode design as an optimization problem that includes all relevant aspects. Recent advances at the spatial scales depicted in Figure 2 foresee such capability in the future. Representations of heterogeneous structures are in this view needed to process the knowledge of the constituent materials and their interfaces gained at the atomic and nano-scale, and from 3D measurements for integration into numerical or analytical analyzes at the mesoscale. Emphasis is placed on capturing the contribution of local geometrical features to the material functionality, while maintaining the computational demand of each procedure in the view of degradation analyzes and assessment of optimization based on morphological and topological manipulations of measured or artificially generated 3D structures.

**3D nanoscale imaging of electrode structures.**— The 3D structure of SOFC materials is commonly measured by serial sectioning using a focused ion beam-scanning electron microscope (FIB-SEM).<sup>17</sup>

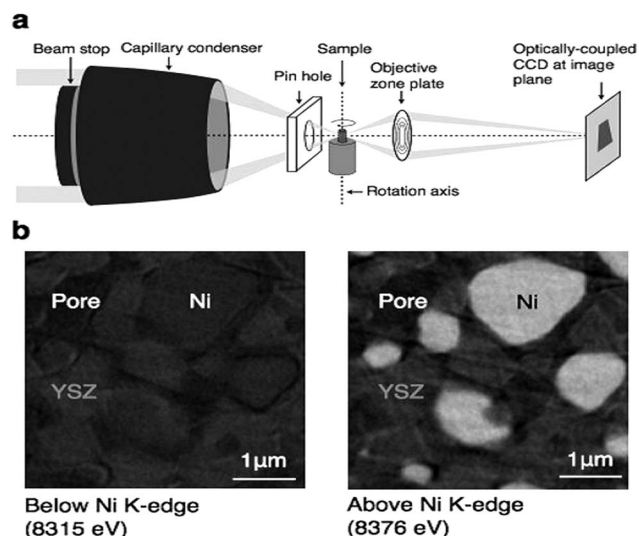


**Figure 4.** (a) Components of transmission X-ray microscope. (b) Illustration of elemental mapping using absorption contrast imaging: slices within the reconstructed XNT data of a Ni-YSZ anode, below and above the Ni K-edge.

X-ray nanotomography (XNT) based on absorption contrast imaging with a full-field transmission X-ray microscope (TXM) has become a viable alternative, thanks to progressive improvements in the spatial resolution, from around 50 nm<sup>18</sup> down to 17 nm recently.<sup>19</sup> It can be applied as well to the analysis of composite MIEC membranes and other energy materials as described in subsequent sections. TXM has several interesting advantages but its use as a spectroscopic tool is limited by the availability of synchrotron X-ray sources.<sup>18</sup> Figure 4 is a schematic view of the arrangement of the main TXM optical elements for XNT. 3D data are obtained by reconstruction, using a filtered back projection or an iterative reconstruction algorithm, from 2D projections gathered during stepwise rotation of the sample over 180°. The number of projections typically varies between hundreds to thousands per energy level depending on the material features and required 3-D spatial resolution. The image quality is significantly increased by producing cylindrical samples by FIB milling to guarantee a uniform cross-section throughout the rotation.<sup>20</sup>

X-ray nanotomography is non-destructive, which makes it possible to track structural changes “in situ” or “in operando” under polarization; to follow critical steps of an SOFC electrode during manufacturing processes; or to follow the reduction process of a Ni-YSZ anode before operation and after reduction-reoxidation cycling. Our approach for heterogeneous materials representation has been developed to effectively process such data. Near edge differential absorption imaging enables elemental mapping of either the desirable or detrimental formed phases, within the limits of X-ray source, as shown in Figure 4.<sup>21</sup> X-ray absorption near edge structure (XANES) spectroscopy can further enhance detection sensitivity and provide the knowledge of the oxidation state of the elements.<sup>22</sup> This approach can potentially provide the 3D distribution of the oxidation state of transition metals in common MIEC cathode materials, such as Co or Fe in LSCF, but its deployment practically remains challenging and currently limited to averaged measurements under the conditions of SOFC cathode operation.<sup>23</sup> The section on Meso-design for Charge Storage and Polarization Management provides the details of the imaging parameters for XNT of a single solid phase MIEC material.

*Deterministic geometric representations of heterogeneous structures for electrode structure optimization based on morphological and topological manipulations.*— The representation of a heterogeneous electrode material structure provided by skeleton-based partitioning is currently evaluated in the view of electrode design. The methodology is based upon the topological information provided by a

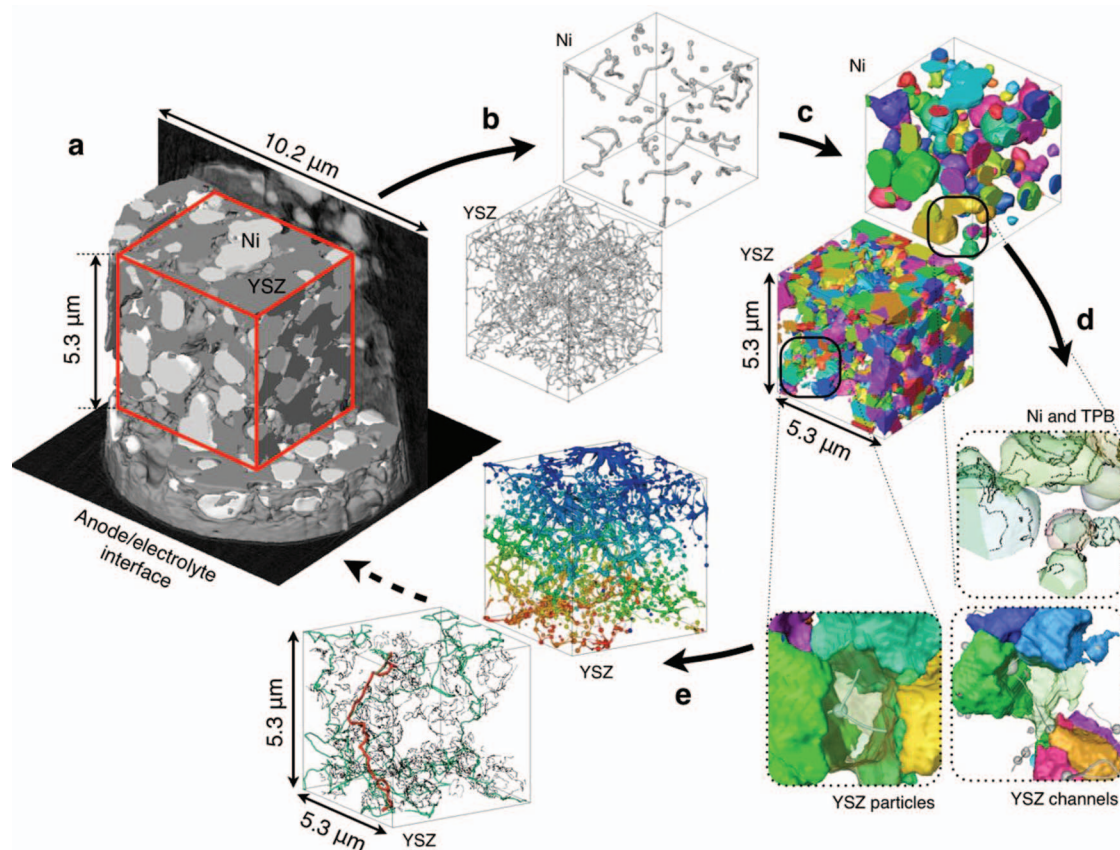


**Figure 5.** Process to generate a digital structure from a real SOFC electrode (Ni-YSZ anode) (a) Reconstruction of the X-ray nanotomography data of a cylindrical sample produced by FIB to generate a grayscale digitized dataset (shown by the ortho-slice), which is then thresholded to produce a digitized volume element representing the distinct phases (Ni, YSZ, pore) of the electrode. A region of interest (ROI, red frame) is extracted for further analysis. (b) The ROI is thresholded for each phase and skeletonized (only YSZ and unconnected Ni, for this specific sample, are shown). (c) Each phase is segmented into channels and particles, which (d) are characterized to yield structural parameters. (e) The structure representation provides the topological and morphological information required by analytical or numerical modeling approaches. Upper view: potential distribution in the YSZ phase provided by an ohmic loss calculation using electrochemical fin theory. Lower view: determination of path between the top and bottom faces that minimize the inverse of the total triple-phase boundary on a particle.

3D skeleton, which describes a phase volume as a set of vertices connected by edges, to partition the structure into particles for analysis of the relationships between geometry and properties of the material. The procedures implemented in Matlab and Avizo are indifferently applicable to multi-phase sample volumes obtained from segmentation of XNT or FIB-SEM data or generated artificially. They have been developed to characterize heterogeneous materials containing percolating phases, purposely added dispersed nanoparticles, or undesirable phases formed in operation because of material instability or contamination. Figure 5 shows the implemented steps in the processing and analysis of XNT data (a) with our partitioning approach (b,c,d) and electrochemical fin modeling approach (e and Section “Meso-design of HeteroFoam SFM material to Manage Polarization in SOFC electrodes”), with the aim of providing guidance for design. Ref. 24 describes in more detail a version of our partitioning approach applied to single-solid phase materials.

The 3D skeleton is first extracted for each phase separately by topological thinning of the distance map,<sup>25</sup> which is intuitively a peeling process to a single voxel thickness (Figure 5b). Operations on the phase volume prior to the calculation of the distance map for skeletonization and further manipulations of the extracted skeleton allow some level of control to generate an appropriate skeleton for partitioning of the structure. Labeling, filling and padding are optionally applied prior to the computation of the distance map to prevent loss of isolated regions and unrealistic partitioning of particles containing inclusions of other phases. The skeleton is then manipulated from

analysis of the connectivity, location, geometry and local thickness evaluated from the distance map value information, of each edge.

### Design of HeteroFoam Membranes

*Function and significance.*— Ceramic membranes which transport oxygen ions play an essential role in a number of energy conversion related systems including oxygen separation and permeation membranes.<sup>26–29</sup> Materials typically used in combustion devices to support oxy-fuel combustion or for partial oxidation reactions involving the production of synthesis gases, require mixed oxygen ion and electronic conduction. MIEC can be achieved in two ways. Either by selecting a material which i) supports both ionic and electronic conduction, or ii) forms a two phase composite of an ionic conductor and an electronic conductor. Selecting an appropriate MIEC is complicated by the fact that it must satisfy a number of challenging criteria. As a permeation membrane, it must i) support a high level of MIEC, ii) catalyze the appropriate reactions at the high and low  $pO_2$  interfaces, iii) remain stable at elevated temperatures under both oxidizing and reducing conditions, iv) retain adequate strength and v) exhibit minimum chemical expansion. In single phase materials, the tailoring of properties including the ratio of ionic conductivity to the material’s electronic conductivity has been accomplished by the introduction of aliovalent doping elements creating point defects which facilitate the diffusion of charged species. Microstructural modifications including grain size effects have also been found to

affect MIEC characteristics.<sup>30,31</sup> The model oxygen ion conducting system CeO<sub>2</sub> displays a drastic increase in electronic conductivity of nanocrystalline samples due to a decrease in the energy required for reduction of nanometer size cerium oxide and space charge effects at the grain/grain boundary interface.<sup>32</sup> Brinkman recently demonstrated the feasibility of utilizing nanocrystalline CeO<sub>2</sub> as an oxygen separation membrane with the microstructural feature of grain size as a design “tool.”<sup>33</sup>

Despite these advances, a comprehensive design methodology taking into account membrane composition, microstructure and morphology has not yet been developed. The approach of many groups, including our own for membrane design is to use dual phase (composite) membranes. The inherent flexibility of multiphase systems makes it more feasible to tune the various properties needed to satisfy the set of stringent chemical, electrical, thermal and mechanical properties of the MIEC. The following sections describe composite MIEC membranes structure, function, traditional characterization and the HeteroFoam approach to membrane design.

**Material property characterization.**— Composite MIEC membranes consist of two contiguous phases, an ion-conducting phase and an electronic conducting phase. In this work, Ce<sub>0.8</sub>Gd<sub>0.2</sub>O<sub>2</sub> was chosen as the ion-conducting phase and CoFe<sub>2</sub>O<sub>4</sub> was selected as the electronic conducting phase. This system has limited reactivity between constituent phases, demonstrates high oxygen flux and stability under reducing environments and serves as a model system for general composite membrane studies.<sup>43</sup> Transport (permeation) of oxygen occurs as a coupled transport of ions and electrons. The overall process is divided into three steps: (a)  $\frac{1}{2}\text{O}_2(\text{g}) + 2\text{e}'(\text{M}) \rightarrow \text{O}^{2-}(\text{I})$  at one surface (Feed), (b) Coupled transport of O<sup>2-</sup> and 2e' in opposite directions through the bulk, and (c)  $\text{O}^{2-}(\text{I}) \rightarrow \frac{1}{2}\text{O}_2(\text{g}) + 2\text{e}'(\text{M})$  at the other surface (Permeate).

The description above is formally described by considering the Wagner description of oxygen flux given in Equation 1.<sup>34</sup>

$$J_{\text{O}_2} = \gamma \cdot \frac{RT}{16F^2L} \cdot \int_{\ln \text{PO}_2'}^{\ln \text{PO}_2''} \frac{\sigma_e \sigma_i}{\sigma_e + \sigma_i} d(\ln \text{PO}_2) \quad [1]$$

where  $J_{\text{O}_2}$  is the permeation flux of gas (O<sub>2</sub> in this case) mol/m<sup>2</sup> s, F is the Faraday constant, R is the gas constant,  $\sigma_e$  and  $\sigma_i$  are the electronic and ionic conductivities and  $\text{PO}_2'$  and  $\text{PO}_2''$  are the gas partial pressure on the oxygen rich and oxygen lean sides of the membrane respectively. The factor  $\gamma$  is derived from the introduction of a “characteristic length,  $L_c$ ” below which the flux does not increase with sample thickness reduction. A schematic depicting oxygen separation membrane functions and principles is displayed in Figure 6. In addition, it is seen that Equation 1 predicts the flux is inversely proportional to the membrane thickness. However, the

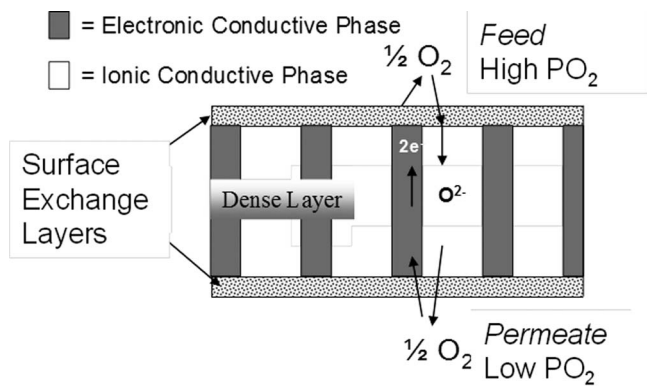


**Figure 6.** Oxygen Separation Membrane: Function and Principle.

actual oxygen flux is also a function of the surface kinetics/oxygen reduction reaction. With decreasing thickness of membranes aimed at higher gas flux, surface and interfacial effects become more important and can dramatically impact membrane performance.<sup>35–37</sup> In typical oxygen separation membranes fabricated from conventional ceramic processing techniques this characteristic length is on the order of 80–100  $\mu\text{m}$ ; however nanocrystalline thin films have demonstrated increased oxygen flux with decreasing thickness down to the <10 microns.<sup>36</sup> Clearly microstructure has an impact on both bulk and surface transport; however the relations governing this behavior have not been established.

**Experimental method.**— The dual phase membranes were prepared by mixing the respective volume percent of the ionic conductive phase Ce<sub>0.8</sub>Gd<sub>0.2</sub>O<sub>2- $\delta$</sub>  (InfraMat Advanced Materials LLC) and the electronic conductive phase CoFe<sub>2</sub>O<sub>4</sub> (InfraMat Advanced Materials LLC) by ball milling powder in ethanol for 6 hours. After drying and sieving, ceramics were mixed with a binder and uniaxially pressed into pellets of 16 mm diameter with a force of 20 kN and sintered at 1300°C for 2 hours in air at a ramp rate of 2°C/minute during heating and cooling stages. Ceramics were characterized from 10 to 90 degrees two theta on a PanAnalytical X-ray diffractometer to determine phase formation. The sintered microstructure and chemical composition were investigated on a Hitachi instrument equipped with Energy Dispersive Spectroscopy (EDS). The conductivity measurements were performed on Pt coated ceramics surfaces. Pt paste, grade 5542 (ESL Inc.) was applied, dried at 110°C for 10 minutes and annealed to 950°C for 10 minutes at with a ramp rate of 5°C/min. The conductivity and dielectric response was measured over a wide temperature range (20°C–1200°C) and frequency (3  $\mu\text{Hz}$ –20 MHz) range in several gas environments using a Novocontrol broadband spectrometer. Gas was provided to the feed and permeate side independently at a flow rate of 50 mL/min with a gold seal used to minimize leakage. The following combinations were used: i) air/air (PO<sub>2</sub> 0.21 atm), ii) N<sub>2</sub>/N<sub>2</sub> (PO<sub>2</sub>  $\sim 10^{-4}$  atm) and iii) Air/N<sub>2</sub>. Combinations i) and ii) were used to determine the oxygen partial pressure (PO<sub>2</sub>) dependence of conductivity at equilibrium conditions. Combination iii) was effectively an in-situ oxygen transport measurement correlating changes in conductivity with oxygen ion and electron migration in the materials due to the gradient in oxygen chemical potential. Oxygen flux measurements were performed by placing the sample between two quartz tubes using a glass ring (melting point 620°C) for gas sealing, and a metal spacer with a diameter of 5 mm to control the area of gas flux. Air at 1 atm was supplied to the bottom of the porous substrate (feed side) while flowing He (20 sccm) was supplied to the permeate side. The gas concentrations of O<sub>2</sub> and N<sub>2</sub> were measured on the permeate side using a gas chromatograph (GC323; GL Sciences Co., Ltd). The leakage of oxygen was calculated by measuring the volume of N<sub>2</sub> gas from air on the permeate side. The oxygen permeation flux was corrected using the total measured oxygen on the permeate side minus the physical leakage of oxygen.

**Results and perspectives.**— The SEM determined microstructure of the 60%CGO–40%CFO composite membrane is displayed in Figure 7. The relatively fine, sub-micron ( $\sim 500$  nm) grain size observed is a consequence of the starting materials particle size of approximately 100 nm. The EDS chemical composition mapping reveals the distribution of the two phases including elemental partitioning at the interfaces resulting in potential Gd-Fe-O crystalline phases. Cation diffusion during fabrication and during long term utilization may impact the performance and stability of the membrane and is a major topic of current interest (Lein, Wiik et al. 2006).<sup>38</sup> Figure 8 displays the oxygen permeability (mol/m s) of the 0.6CGO–0.4CFO composite membrane in this work compared to literature values for ceramic-ceramic and ceramic-metal composite membranes indicating the appreciable oxygen transport at temperatures in the 800–900°C range. All of the flux data utilized in Figure 8 were taken for membranes where bulk diffusion was dominant with thickness greater than 0.5 mm and under similar PO<sub>2</sub> gradients (air feed to inert gas sweep).

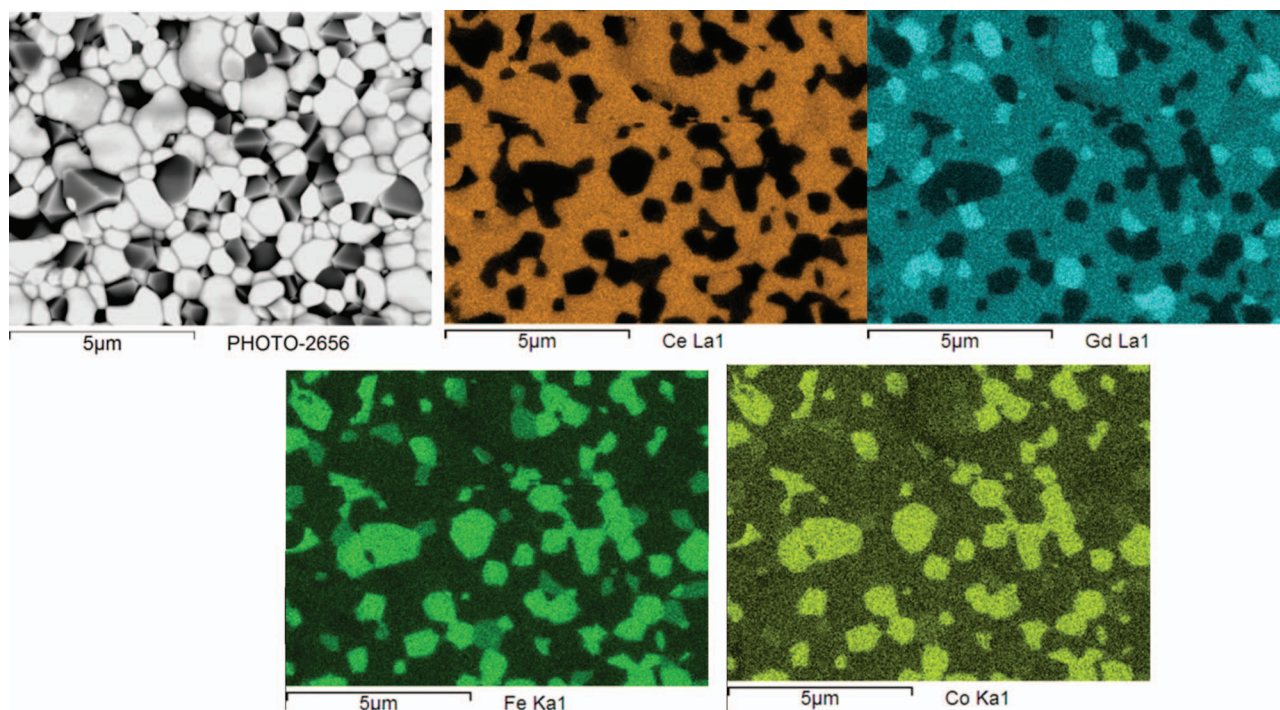


**Figure 7.** 0.6CGO-0.4CFO Sintered at 1300°C for 2 hours SEM-Secondary Electron Image and EDS chemical composition analysis.

Normalized flux values, referred to as the material's permeability ( $\text{mol/m s}$ ) were obtained by taking the product of the oxygen flux with the given membrane thickness. Figure 8 correlates the oxygen flux versus temperature for various ceramic/ceramic and ceramic/metal composite membranes found in literature. Graphical representations of oxygen flux serve as a useful summary of the available data; however they do not function well as a design tool. In addition, little evidence is available on the impact of microstructure and morphology on the bulk and surface oxygen transport. Clearly, a design

methodology is required to tailor membrane composition, microstructure and morphology toward performance requirements for a given application.

Dual phase MIEC membranes are also functional dielectrics that conduct ions or electrons as a function of available conduction species and temperature. Heterogeneous MIECs display conduction characteristics that are also highly dependent on morphology and local geometry. Dielectric materials can be poor conductors of electricity, but are often efficient supporters of electrostatic fields so that their capacitive behavior contains much information about their fundamental character and function. Broadband dielectric spectroscopy (BDS) (with excitation in the  $10^{-6}$  to  $10^{12}$  Hz range) is a robust, well established and well annotated field of science and technology that studies the dynamics of bound (dipole) and mobile charge carriers as a function of applied conditions.<sup>54</sup> The present work attempts to use that foundation to establish the effect of morphology and local interfaces on MIEC functionality in membranes.

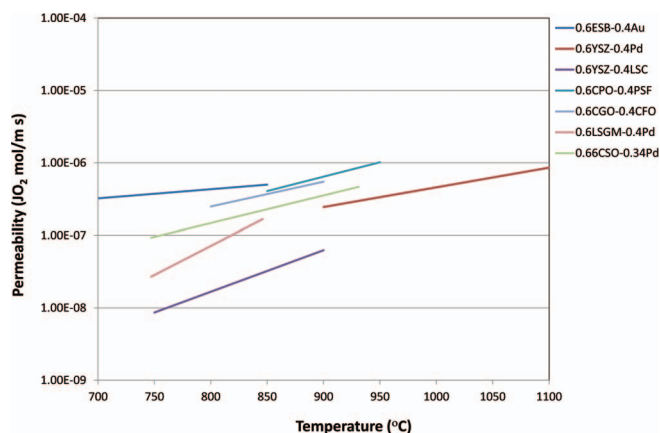


**Figure 8.** Oxygen permeability ( $\text{JO}_2 \text{ mol/m s}$ ) versus temperature ( $^{\circ}\text{C}$ ) for select dual phase materials: 0.6CGO-0.4CFO = 60%  $\text{Ce}_{0.8}\text{Gd}_{0.2}\text{O}_2$  and 40%  $\text{CoFe}_2\text{O}_4$  (This Work); 0.6ESB-0.4Au = 60%  $(\text{Bi}_2\text{O}_3)_{0.75}(\text{Er}_2\text{O}_3)_{0.25}$  and 40% Au (Chen, Kruidhof et al. 1996)<sup>63</sup>; 0.6YSZ-0.4Pd = 60%  $(\text{ZrO}_2)_{0.94}(\text{Y}_2\text{O}_3)_{0.06}$  and 40% Pd (Chen, Boukamp et al. 1995);<sup>64</sup> 0.6YSZ-0.5LSC = 60%  $\text{Zr}_{0.8}\text{Y}_{0.2}\text{O}_2$  and 40%  $\text{La}_{0.8}\text{Sr}_{0.2}\text{CrO}_3$  (Wang, Zhan et al. 2006);<sup>65</sup> 0.6CPO-0.4PSF = 60%  $\text{Ce}_{0.9}\text{Pr}_{0.1}\text{O}_2$  and 40%  $\text{Pr}_{0.6}\text{Sr}_{0.4}\text{FeO}_3$  (Luo, Jiang et al. 2012);<sup>29</sup> 0.6LSGM-0.4Pd = 60%  $\text{La}_{0.8}\text{Sr}_{0.2}\text{Ga}_{0.83}\text{Mg}_{0.17}\text{O}_3$  and 40% Pd (Huang, Schroeder et al. 1999);<sup>66</sup> 0.66CSO-0.34Pd = 66%  $\text{Ce}_{0.8}\text{Sm}_{0.2}\text{O}_2$  and 34% Pd (Huang, Schroeder et al. 1999).<sup>66</sup>

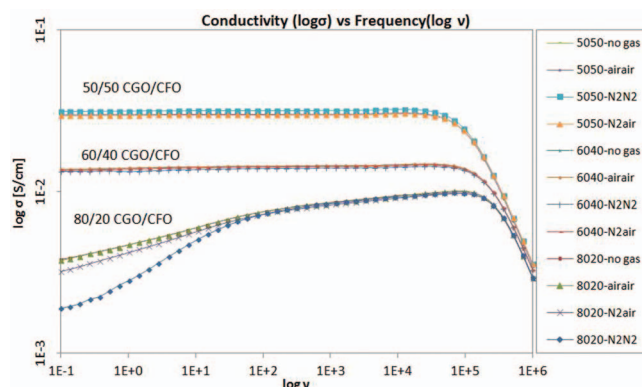


**Figure 9.** BDS Conductivity versus Frequency at various gas flows at 800°C for 50/50, 60/40, and 80/20 volume% CGO/CFO.

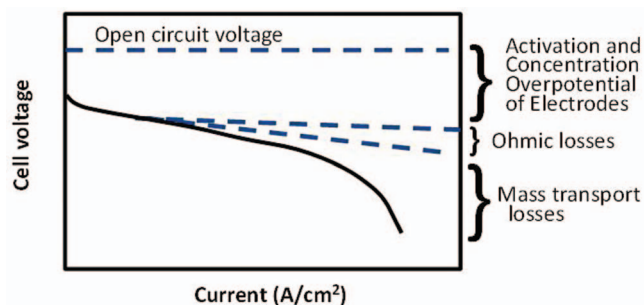


**Figure 10.** Schematic of polarization effects in an operating fuel cell.

Figure 9 presents the BDS determined conductivity versus frequency and oxygen partial pressure driving force for three different mixtures of CGO-CFO. An increase in total conductivity with an increase in the volume fraction of the electronic conductive phase (CFO) is observed. From Equation 1, an increase in the electronic conductivity should lead to an increase in the oxygen flux if the ionic conductivity of the mixture is maintained bulk oxygen diffusion is dominant. However, as we further increase the volume fraction of electronic conductive material, we concomitantly reduce the fraction of material available for oxygen ion conduction which leads to a reduction in oxygen transport. In addition, the concept of volume fraction of a given material is misleading and imprecise for the present case; one could envision a microstructure design with a thin, contiguous electronic conductive phase extending across the membrane thickness. This could result in a composite membrane with a low volume fraction of electronic conductor possessing a larger total conductivity than alternative microstructures. From the preceding discussion, there arises a need to develop a new framework for membrane design taking into account the microstructure, interfacial and emergent properties of MIEC materials.

*The HeteroFoam approach for membrane design.*— Dense composite membranes provide a convenient starting point for the development of multiphysics models. Measurements of transport properties including oxygen flux, and constituent material properties such as permittivity and conductivity as a function of material composition and microstructure can be directly incorporated into the modeling effort in order to guide the design of optimal heterogeneous functional materials in the following manner.

Dual phase membranes like those presented in Figure 7 with varying volume fraction, microstructure and morphology are currently being fabricated by varying the annealing temperature and sintering rate of non-equilibrium densification techniques such as Spark Plasma Sintering (SPS).<sup>39</sup> The resulting microstructure will be evaluated the X-ray nanotomography (XNT) synchrotron technique to get the 3D structure of “dual phase” membranes. Comsol simulations with the XNT determined microstructure will be performed using the individual material constituent properties (conductivity, permittivity) determined from BDS analysis under the appropriate boundary conditions including varying oxygen partial pressure. The predicted “composite” membrane performance will be compared with the experimentally determined properties (conductivity, flux) with differences analyzed in terms of emergent properties and interface contributions. These results as a function of volume fraction of mixtures and microstructure can be used to develop a modified Wagner equation with microstructural variables. An oxygen flux model will be developed and validated with several dual phase compositional and morphology variations. This model will be used to predict the optimal composition, and morphology for a given material system. This approach of using atomic level inputs and intrinsic single phase materials properties combined with actual microstructure and measurements enabling the output of constitutive “properties” of the dual phase system that can be used in global balance equations such as the Wagner relation for oxygen

flux is the essential feature of HeteroFoam material design concept and is graphically depicted in Figure 2 describing HeteroFoam as a foundation concept. This work is in progress.

### Meso-design for Charge Storage and Polarization Management in Heterogeneous Functional Materials

Fundamentally, every heterogeneous material is dielectric. Unless the conductivity and permittivity of adjacent phases are identical, individually and respectively, there is a disruption of charge transfer at the boundaries and some internal polarization. The consequences of this pervasive effect are profound and fundamental to the design of heterogeneous material systems. This is especially true when the constituents are functional, i.e., when they operate on the applied fields in some way. Electrochemical activity, diffusion driven by chemical potentials, and many conduction mechanisms are examples of such functionality.

*Non-faradaic polarization and charge storage.*— “Polarization curves” are universally used to describe the operation of fuel cells. They provide a useful measure of the quality of a given fuel cell, with largely non-specific information about the reasons for the limitations on that performance.<sup>40</sup> Figure 10 shows a typical schematic example of such a curve, although it should be noted that the features depicted there are not universal. Heterogeneity of materials is a major driver for the losses observed in such a characterization, perhaps second only to activation losses. This device-specific illustration identifies two important observations in the present general context. Since heterogeneity is a design parameter, it is important to understand and control the losses driven by heterogeneity in such systems, and, in other cases, it is perhaps more important to understand how to design heterogeneity to exploit its capability to create polarization to store charge and energy (one of the grand challenges of our times).

To isolate that discussion, we consider the non-faradaic aspects of the effect of heterogeneity on charge storage and polarization. In fact, there is a strong foundation of earlier work to support this discussion.<sup>41,42</sup> Figure 11 illustrates this distinction, from some of our earlier work.<sup>43</sup> For an operating SOFC, the polarization losses increase with operating time, as shown in Fig. 11a, as expected. For that same cell, measurements of the capacitance were made with nitrogen flowing on the anode and no current flowing through the cell; all other operating conditions were maintained. The results of the capacitance measurements are shown in Fig. 11b. Two aspects of the results are particularly striking. First, the magnitude of the capacitance of this small button cell is remarkably large; the units on the ordinate of Fig. 11b are in Farads. Indeed, every fuel cell is a capacitor; if it were not, we would have no current through the external circuit. Second, the magnitude of the non-faradaic changes in capacitance of the fuel cell associated with the polarization changes are large, nearly half an order of magnitude on that logarithmic plot. So while the performance of the fuel cell is changing by a fraction, the non-faradaic polarization is changing by a factor. The common feature at the foundation of these observations is the effect of variations in the nano- to meso-heterogeneity of these materials during service. This remarkable sensitivity of non-faradaic dielectric response to local morphology has been noted in another context in earlier publications.<sup>44</sup>

Our present purpose is to show that there is a strongly emergent character to dielectric charge storage in heterogeneous materials, and that the science foundation for this is based on local field interactions in some cases. To demonstrate this feature, we use a closed form, embedded boundary method developed in our laboratory to calculate the local surface charge stored at the boundaries of an “inside” phase embedded in an “outside” matrix. Further, we take advantage of the robustness of this approach to consider non-dilute solutions of such particles for which the included phase particles have boundaries arbitrarily close to the representative volume elements, so that neighboring particles create local fields that interact with each other,

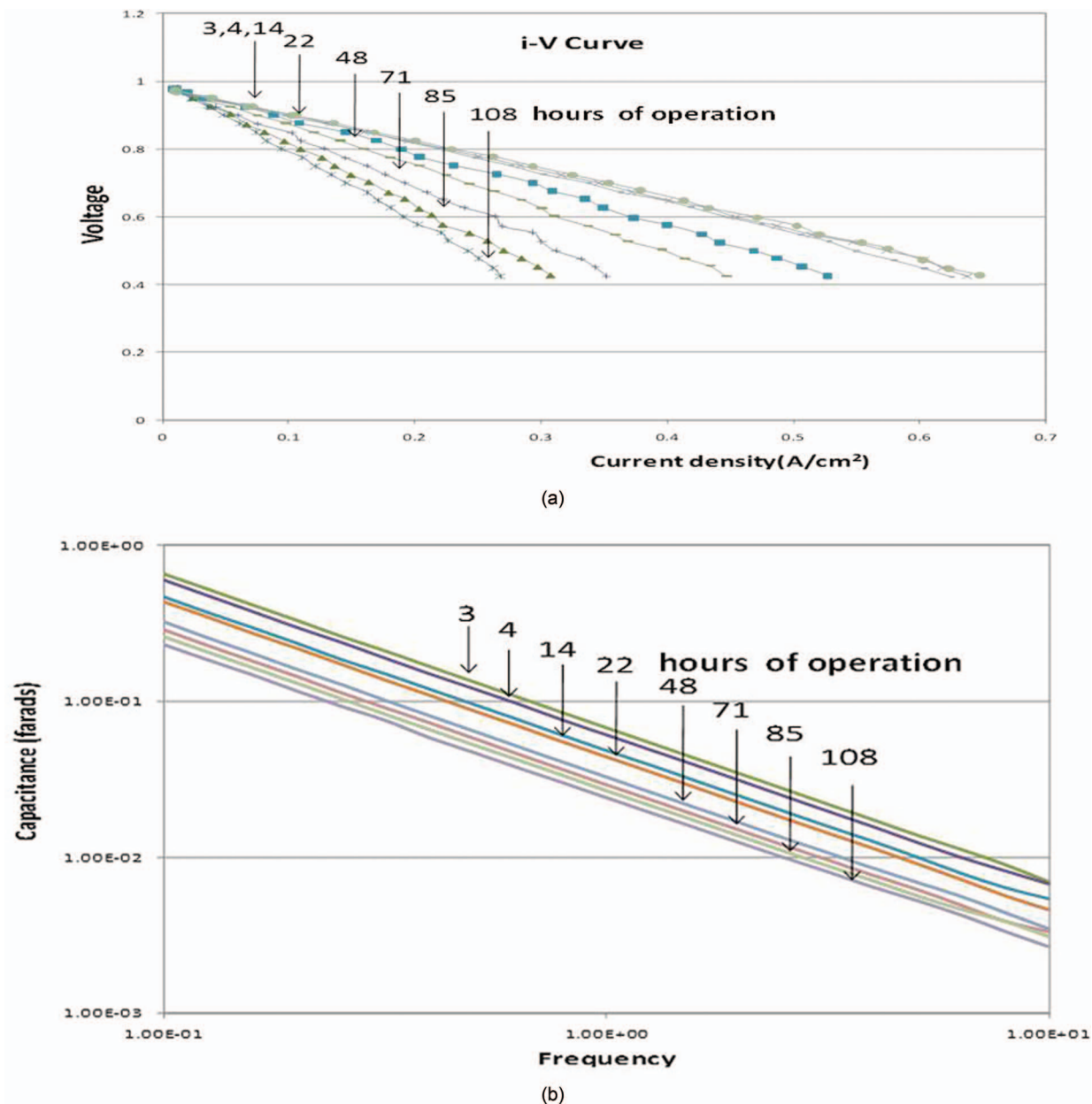


Figure 11. Polarization curve for an SOFC cell (a) measured after several hours of operation, and non-faradaic capacitance measured after each period (b).

i.e., we are able to create a heterogeneous material with interacting particles in the presence of an applied electric field. A summary of the formulation follows.

Consider the physical problem in which a dielectric particle is immersed in a continuous phase in a general AC electric field. The continuous phase (dispersion medium) has an arbitrary dielectric constant  $\epsilon^o$  and conductivity  $\sigma^o$ , where the superscript “o” represents “outside” of the particle, while the dielectric particle has an arbitrary dielectric constant  $\epsilon^i$  and conductivity  $\sigma^i$ , where the superscript “i” represents “inside” the particle. Linear isotropic homogeneity is assumed for both the continuous phase and the particles. For a sinusoidal steady-state electric field, the phasor  $V$  of the potential inside and outside of the particle with specified conductivity, permittivity, and frequency is governed by the complex Laplace’s equation

$$\nabla^2 \tilde{V}(x, y, z) = 0 \tag{2}$$

with corresponding interface conditions

$$\tilde{V}^o = \tilde{V}^i, \quad \tilde{\epsilon}^o \frac{\partial \tilde{V}^o}{\partial n} = \tilde{\epsilon}^i \frac{\partial \tilde{V}^i}{\partial n} \tag{3}$$

where

$$\tilde{\epsilon}^i = \epsilon + \frac{\sigma}{i\omega} \tag{4}$$

For solutions of the potential field having the form

$$V(x, y, z, t) = \text{Re}\{\tilde{V}(x, y, z) \exp(i\omega t)\} \tag{5}$$

the total interface charge density can be written as

$$\sigma_t = -\frac{\partial V^o}{\partial n} + \frac{\partial V^i}{\partial n} \tag{6}$$

The general spectral analytical solutions outside and inside of a circular dielectric particle can then be written as

$$\tilde{v}^o = \tilde{b}^o + \sum_{n=1}^{\infty} \left[ 1 + \tilde{K} \left( \frac{r_p}{r} \right)^{2n} \right] r^n (\tilde{a}_n \cos n\theta + \tilde{b}_n \sin n\theta) \quad [7]$$

$$\tilde{v}^i = \tilde{b}^o + \sum_{n=1}^{\infty} \frac{2\tilde{\epsilon}^o}{\tilde{\epsilon}^o + \tilde{\epsilon}^i} r^n (\tilde{a}_n \cos n\theta + \tilde{b}_n \sin n\theta) \quad [8]$$

where the factor  $\tilde{K} = \frac{\tilde{\epsilon}^o - \tilde{\epsilon}^i}{\tilde{\epsilon}^o + \tilde{\epsilon}^i}$  and  $r_p$  is the particle radius, yielding the total interfacial charge density in the form

$$\sigma_t = \sum_{n=1}^{\infty} 2nr_p^{n-1} [\text{Re}(\tilde{K}\tilde{a}_n\tilde{S}) \cos n\phi + \text{Re}(\tilde{K}\tilde{b}_n\tilde{S}) \sin n\phi] \quad [9]$$

The authors have presented a general spectral method for finding solutions to this equation set for various geometries.<sup>45-47</sup> Solutions for circular, and elliptical particles having various orientations to the applied vector electric field were found, and the extreme sensitivity of those results to the local geometry and orientation of the particles as well as to their relative conduction and permittivity values was investigated.

One example of the results of that study is shown in Fig. 12 (for circular particles). For that example, a matrix that has very low con-

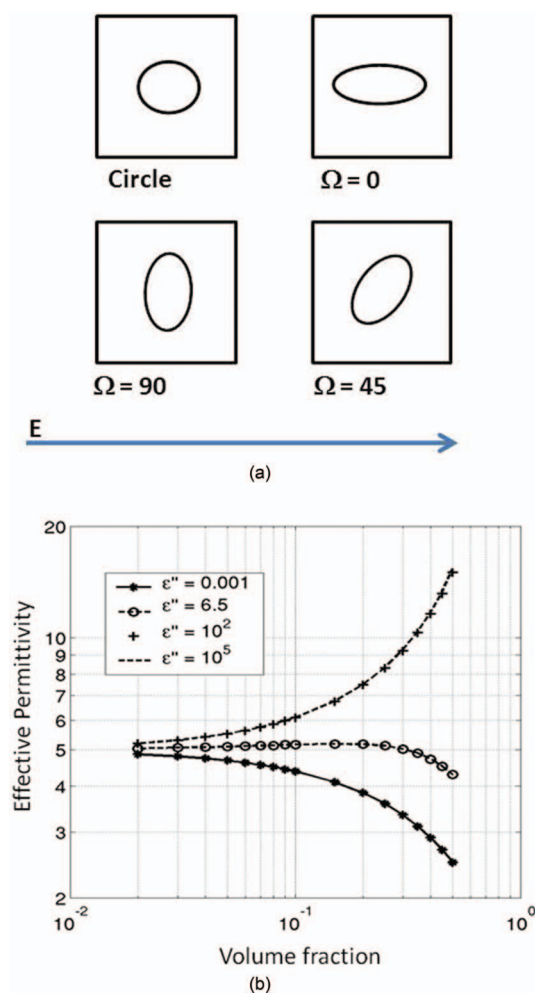


**Figure 12.** Representative volume elements (a) used for the Physalis solution method to determine local charge storage and effective permittivity in non-dilute heterogeneous dielectric materials,<sup>67-69</sup> and HeteroFoaM effective permittivity (at 10 Hz) predicted for different constituent properties (b) showing emergent property characteristics.

ductivity and significant values of permittivity (of the order of 6), and included particles having small but significant conduction with permittivity varied over several orders of magnitude were considered for the results shown in Fig. 12. (These values were chosen to facilitate experimental validation using epoxy matrix materials with variable densities of microcracking in moist environments.) For small values of second phase (up to 10 percent or so for this example), variations in global (effective) permittivity were small, but as one would expect, inclusions with very large permittivity increased the global value, while those with vanishing permittivity caused decreases. However, as one approaches situations in which the particles come very close to each other (0.634 volume fraction for the monodisperse assumption and 0.74 for a close-packed arrangement), the global property changes dramatically, and begins to take on extreme values, especially when the included phase is highly dielectric. It should be emphasized that there is no conduction between particles in this problem; they are not allowed to touch each other. The emergence of extreme values of global permittivity is associated only with the interactions of the local fields created by charge storage at the boundaries of the particles. In a fuel cell, these local polarizations can be detrimental if they interfere with conduction, as shown in Fig. 10. In the case of capacitors, such extreme permittivities can provide a very effective way of storing energy. A model which captures the local constituent interactions, such as the one outlined above, is an essential tool for the design of heterogeneous material systems to manage charge storage and transport.

*Emerging properties in HeteroFoaM systems.*— The final point to be made in this sub-section is that the emerging property effects shown in Fig. 12 must be understood and modeled on the basis of the physics that drives the local interactions in these material systems. “Mixture” equations or other “effective property” approaches are insensitive to exactly the local effects that control and generate such emergent results.<sup>48</sup> In the present context, much has been written about using effective property or ‘mixing laws’ to represent the effective permittivity of heterogeneous materials. El Bouazzaoui, et al., discuss the limitations of such attempts in the context of the well-known Wiener’s bounds derived for the harmonic and arithmetic means of the intrinsic permittivities.<sup>49</sup> Such discussions are limited to volume fractions of second phase that preclude local interactions and resulting emergent properties. But emergent behavior is easily demonstrated for even simple situations. The data in Fig. 13 were recorded in our laboratory for 40 μ carbon flake material embedded in epoxy with various volume percent concentrations. Such non-dilute mixtures show sharply emergent properties, not bounded by the intrinsic constituent values, as demonstrated by those data. It should be mentioned that the real part of the conductivity of the 30% mixture is still of the order of 10<sup>-7</sup> S/cm, well below a “conduction threshold.”

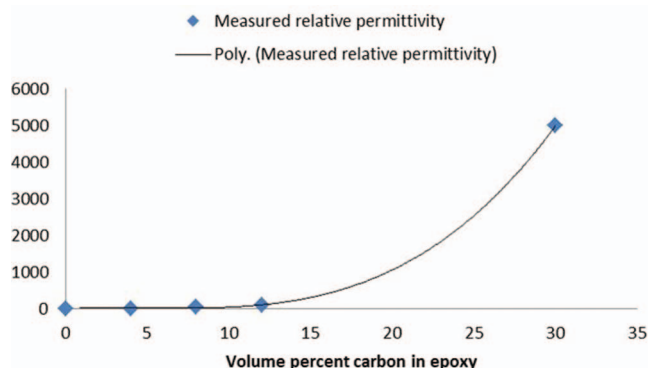


**Figure 13.** Measured composite permittivity of carbon flakes embedded in epoxy matrix for increasing volume percent.

**Meso-design of HeteroFoams to manage polarization in electrodes.**— The meso-design of heterogeneous electrode materials for energy conversion or storage devices, such as fuel cells or batteries, focuses on the understanding of long-term polarization resistance under the diverse local conditions found in the system, within the constraints of ensuring the mechanical integrity of the layer. This task requires the knowledge of how, at any of the space scales depicted in Figure 2, choices in the materials and their arrangement forming the heterogeneous structure, govern the behavior of a heterogeneous structure.

The recent advances of 3-D imaging techniques have promoted the rapid increase of such studies based on 3-D simulations on the geometry measured by X-ray nanotomography using a transmission X-ray microscope or serial sectioning using a focused ion beam-scanning electron microscope. 3-D simulations potentially provide the most detailed insight into the effects of the material morphology and topology on the polarization resistance.<sup>50,51</sup> This is obtained at the cost of computational demands that hinder the use of these approaches (i) at scales of interest to apprehend the electrode as part of the multilayer system in a SOFC, and (ii) for predictive degradation analyzes that require further discretization in time. Methodologies for meso-design do not have to achieve the highest level of local accuracy under given assumptions. They must ensure that the dominant phenomena are included in the analysis and treat geometrical and compositional adjustments of the heterogeneous material together. Therefore, flexibility in retrieving the knowledge gained at the other scales, adequate sensitivity to geometrical effects and capability to provide guidance within shorter time are required. This challenge warrants the development of specific approaches for rapid predictions of the polarization resistance of heterogeneous materials.

Several models for polarization resistance predictions are available in the literature. One class is built upon the analogy in the governing equations that describe heat transport and charge transport in extended surfaces.<sup>8,52-55</sup> A recent study of this kind has focused on the balance between transport in the bulk and surface reaction in structures with variable cross-sections.<sup>52-55,70</sup> Closed form analytical solutions exist for specific profiles, e.g. conical, spherical, exponential, hyperbolic or sinusoidal.<sup>56</sup> The simplification of the electrode structure as a periodic assembly of such elementary building blocks (see insert in Figure 14) provides the basis for analyzing the effects of simple microstructure modifications, in the light of dimensionless parameters and performance metrics similar to those applied in thermal fin analysis. This approach allows identifying regimes resulting from the trade-off between the beneficial increase of the area available for surface charge transfer reaction and the detrimental effect on bulk transport due to constrictions arising from the subsequent variation of the cross-section. Figure 14 depicts the fin efficiency as a function of the resistivity ratio, for different periodic arrangements of conical frustums. The fin efficiency is the ratio of the total current conducted by the fin to the ideal one corresponding to a uniform potential distribution within the fin, whereas the resistivity ratio is the ratio between conductive resistance within the fin and resistance to surface charge transfer. In regime A, the dominance of surface reactions result in high fin efficiency, which indicates that electrode performance would benefit from the creation of additional external surface area before the penalty caused by constrictions in charge diffusion transport prevail. Low fin efficiencies in regime C reflect the opposite undesirable situation. Structure design should therefore aim at regime B in Figure 14, where surface charge transfer reaction and bulk transport effects are balanced. The resistivity ratio can be adjusted by modifying alone or together, the shape structure, the material or its composition. The candidate combinations of shapes and compositions can then be evaluated further from separate analyzes of e.g. their long-term chemical and mechanical stability, under the uneven and evolving local conditions typically found in energy conversion devices. Figure 14 illustrates the range corresponding to LSCF and LiFePO<sub>4</sub>, two typical cathode materials for SOFC and Li-ion battery cathodes, respectively, and TiO<sub>2</sub> a photoelectrode material for dye-sensitized solar cells, using data from the literature.<sup>57-60</sup> This approach therefore provides location-

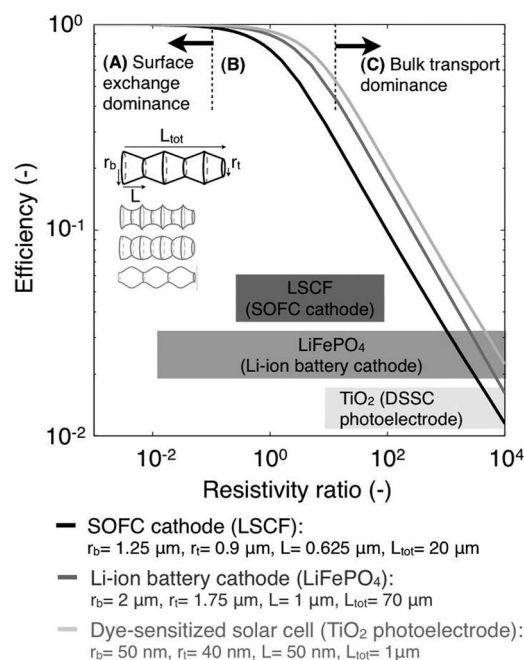


**Figure 14.** Fin efficiency as a function of resistivity ratio for SOFC cathode, Li-ion battery cathode, and dye-sensitized cells represented by periodic assemblies of one profile type for which analytical solutions exist (conical frustums). The grayscale bars indicate the approximate range in resistivity ratio, hence accessible regime, for the typical materials used for these systems.

dependent guidance for specifying together the material and geometry of any functional structure where such trade-off exist, within practically negligible computation time. Refs. 67, 69, and 70 provide the details of its applications to SOFC electrodes, Li-Ion battery cathodes and dye-sensitized solar cells.

The analytical electrochemical fin modeling approach is not restricted to electrode performance analysis based on periodic structures. The building blocks for which analytical solutions exist can serve as a library of building blocks to treat real microstructures measured by XNT or FIB-SEM, with the support of a structure representation provided by partitioning each phase volume based on the skeleton edges (see Figure 15 for illustration). The morphological analysis of the individual particles supports assigning a type within the analytical solution library or proceeding with further partitioning, if required. The adequate set of metrics for this task is yet to be determined and the subject of ongoing efforts. Investigated candidates span from the surface area to volume ratio to curvature analyzes, through investigations of the cross-sections along the skeleton points and measured intra-phase interfacial contact areas. The polarization resistance is computed from the resolution of the resistive circuit problem defined by the network topology. The benefits of intentional gradual compositional changes can be assessed by assigning material properties to each particle separately. The same approach can be used for identifying and understanding the contributions to the polarization losses with higher accuracy or for degradation analyzes. The methodology is currently tested for the case of a single solid phase mixed ionic-electronic conducting electrode made of SrFe<sub>0.8</sub>Mo<sub>0.2</sub>O<sub>3- $\delta$</sub>  (SFM),<sup>61</sup> before extension to multi-solid phase heterogeneous materials. SFM is a perovskite that can serve as either SOFC anode or cathode material, owing to its stability in both oxidizing and reducing environment and adequate electrocatalytic activity for oxygen reduction and hydrogen oxidation. Ref. 61 provides the details of the symmetrical cell fabrication, conductivity, surface exchange coefficient and polarization resistance measurements using electrochemical impedance spectroscopy (EIS). Cylindrical samples of the porous material with a diameter of approximately 10  $\mu\text{m}$  and a height of approximately 20  $\mu\text{m}$  were extracted from the symmetrical cell by a FIB

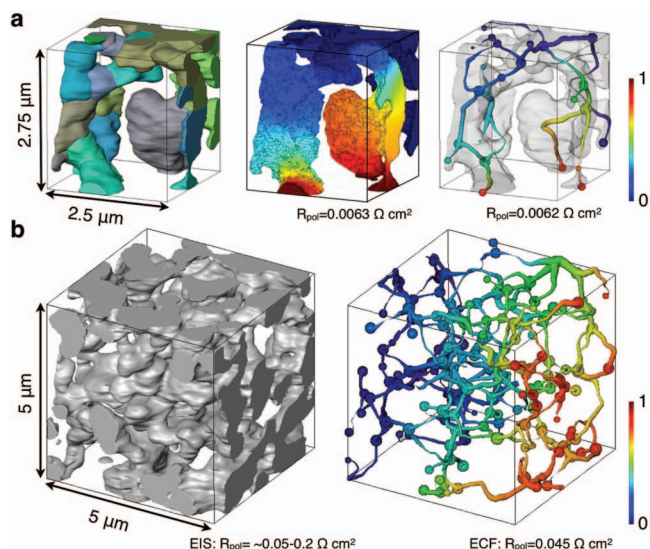


**Figure 15.** Illustration of the coupling between the analytical electrochemical fin and heterogeneous structure partitioning approach for analyzing the polarization resistance of  $\text{SrFe}_{0.8}\text{Mo}_{0.2}\text{O}_{3-\delta}$  electrodes. (a) Partitioned sample volume made of  $100 \times 100 \times 110$  voxels ( $2.5 \times 2.5 \times 2.75 \mu\text{m}$ ) (left), and comparison between the polarization resistance and dimensionless potential distribution computed by electrochemical fin theory (right) and the finite element method (middle). (b) Left: View of a sample volume made of  $200 \times 200 \times 200$  ( $5 \times 5 \times 5 \mu\text{m}$ ) and range in polarization resistance measured by EIS for such material. Right: Polarization resistance and dimensionless potential distribution within the volume, computed by the electrochemical fin modeling approach. The thickness of the skeleton edges corresponds to the local thickness computed from the distance map.

preparation technique.<sup>20</sup> Absorption contrast imaging was performed on the TXM at beamline 32-ID-C at the Advanced Photon Source (Argonne National Laboratory). In contrast to the case of multi-solid phase materials,<sup>21</sup> XNT measurements were carried out at an energy of 8000 eV, which is sufficient to identify the solid SFM phase. The 3-D data were obtained after reconstructed from the 181 projections collected over  $180^\circ$  and watershed-based segmentation to distinguish the solid SFM from the pore phases. Two sample volumes of  $5 \mu\text{m}$  per side (200 voxels) were further extracted and partitioned for ECF and finite-element (FE) analyzes.

A particle by particle comparison between the predictions from the ECF approach and 3-D FE simulations was performed on a sub-volume consisting of  $100 \times 100 \times 110$  voxels ( $2.5 \times 2.5 \times 2.75 \mu\text{m}$ ) partitioned into 24 particles (Figure 15a) and the polarization resistances computed by the ECF approach for the two sample volume of  $5 \mu\text{m}$  per side were compared with the polarization resistance measured by electrochemical impedance spectroscopy (EIS) in Figure 15b. The results show that, already at the current early stage of development, reasonable agreements can be achieved without any specific parameter adjustment and that microstructural effects at a particle level are captured in the analysis.<sup>24</sup>

The ECF approach provides decisive advantages in terms of computational demand.<sup>24</sup> The memory requirement for the SFM sample volume of  $5 \mu\text{m}$  per side is in the range of three to four orders of magnitude smaller than that of 3-D FE simulations ( $\sim 6.5$  GB RAM), whereas the solution time is about one order of magnitude lower. Test cases using the YSZ phase structure in a LSM-YSZ sample of  $5 \mu\text{m}$  per side<sup>62</sup> comprising more than 15000 particles are completed within seconds on a standard desktop computer (dual core 3.2 GHz, 8 GB RAM). Such sample volume could not be processed by 3-D FE with our standard resources (24 GB RAM). Fast, yet accurate predictions are of crucial importance for integration into systematic approaches for rational material design based on science spanning from the nano- to the meso-scale. Computation times below a few minutes allow for compatibility with optimization procedures based on manipulations

of the heterogeneous structure representations and predictive degradation analyzes to characterize the contribution of the morphology and topology to the intrinsic long-term stability of a heterogeneous material.

### Conclusions and Directions for Continued Work

We have identified a new genre of heterogeneous functional materials which we call HeteroFoaM. The genre embraces and represents a class of multi-phase heterogeneous materials designed for concomitant electrochemical, thermal, and mechanical functionality. That genre forms a foundation for the rational design of multiphysics functionality across many scales of time and length to achieve prescribed performance in energy conversion and storage systems.

The essence of “HeteroFoaM” is the concept of using heterogeneous functional material systems as a “meso-material” in the global balance equations for applications such as fuel cells, membranes, and charge storage devices. Our approach is to replace material constants in the global balance equations with constitutive equations that properly combine the properties, morphologies, and (especially) the interactions of the nano/micro-constituents as a function of thermal, electrical, mechanical, and chemical applied fields, to capture the emergent properties that distinguish this genre of materials. The major motivation for this approach is the failure of effective property and mixture equations to capture not only the local physics of those constituent interactions, but also the critical influence of extrinsic factors such as shape, size, and geometry of local morphologies. If done correctly, the applied fields appear in the resulting HeteroFoaM “properties” at the meso-level, and resulting emergent properties such as mixed conduction, extreme values of permittivity, and morphology evolution can be predicted for specified operating conditions at the global level. In that sense, creating the science necessary for HeteroFoaM as a discipline creates the critical bridge required to carry atomic level science to the prediction of macro-level performance to create a knowledge based material design philosophy for the design of energy conversion and storage materials.

Hence, the creation of the HeteroFoaM concept as a genre of heterogeneous functional materials provides a foundation for the design of material systems, by framing a meso-scale problem that uses atomic and nano-scale properties in constitutive equations that represent meso-scale characteristics which then appear in the global balance equations for mass, momentum, energy and charge commonly used to create devices such as fuel cells, batteries, capacitors, and separation membranes. We have presented only a few examples of this sequence in the present paper. Much more is yet to be done, but our work to date demonstrates the utility of the methodology.

### Acknowledgments

This work was presented as a Keynote lecture at the symposium on “Renewable Fuels from Sunlight and Electricity,” PRiME 2012/222nd Meeting of the Electrochemical Society, Honolulu, HI, October 7–12, 2012. The authors gratefully acknowledge the support of the Energy Frontier Research Center for Heterogeneous Functional Materials, the HeteroFoaM Center, for support of this research under DoE grant no. DE-SC0001061 from the Office of Basic Energy Sciences. The X-ray tomography elements of this research were carried out at the Advanced Photon Source (Dr. S. Wang) supported by the U.S. Department of Energy, Office of Science, Office of Basic Energy Sciences, under contract No. DE-AC02-06CH11357, and at the National Synchrotron Light Source (Dr. J. Wang, Dr. K. Chen-Wiegart) at Brookhaven National Laboratory supported by the U.S. Department of Energy, Office of Science, Office of Basic Energy Sciences, under Contract No. DE-AC02-98CH10886. SFM samples were provided by Prof. F. Chen (University of South Carolina) and Ni-YSZ samples were provided by MER Dr. J. Van herle (Ecole Polytechnique Federale de Lausanne, Switzerland). The oxygen membrane characterization elements of this research were carried out at the Savannah River National Laboratory

(Dr. K. Brinkman) which operates under contract No. DE-AC09-08SR22470 with the Department of Energy.

## References

- A. B. Muñoz-García, M. Pavone, and E. A. Carter, *Chem. Mater.*, **23**, 4525 (2011).
- A. B. Muñoz-García, D. E. Bugaris, M. Pavone, J. P. Hodges, A. Huq, F. Chen, H.-C. zur-Loye, and E. A. Carter, *J. Am. Chem. Soc.*, **134**, 6826 (2012).
- S. C. Ammal and A. Heyden, *JPC Lett.*, **3**, 2767 (2012).
- L. S. Yang, S. Chen, Y. Ding, Z. Wang, and M. Liu, *Nano Lett.*, **12** (2012).
- M. K. Song, S. Cheng, H. Chen, W. Qin, J. Bai, T. Tyson, N. Yang, S. Xu, A. Bongiorno, and M. Liu, *Nano Lett.*, under review.
- C. Daan, Y. Du, K. Reifsnider, and F. Chen, *J. Power Sources*, **196**, 6293 (2011).
- M. J. Jørgensen and M. Mogensen, *Journal of The Electrochemical Society*, **148**(5), A433 (2001).
- P. Costamagna, P. Costa, and V. Antonucci, *Electrochimica Acta*, **43**(3–4), 375 (1998).
- D. Bouvard and F. Lange, *Acta Metallurgica et Materialia*, **39**(12), 3083 (1991).
- D. Chen, Z. Lin, H. Zhu, and R. J. Kee, *Journal of Power Sources*, **191**(2), 240 (2009).
- J. Deseure, L. Dessemond, Y. Bultel, and E. Siebert, *Journal of the European Ceramic Society*, **25**(12), 2673 (2005).
- Q. Liu, X. Dong, G. Xiao, F. Zhao, and F. Chen, *Advanced Materials*, **22**, 5478 (2010).
- L. Schneider, C. Martin, Y. Bultel, L. Dessemond, and D. Bouvard, *Electrochimica Acta*, **52**(9), 3190 (2007).
- F. Tietz, A. Mai, and D. Stöver, *Solid State Ionics*, **179**, 1509 (2008).
- H. Yokokawa, H. Tu, B. Iwanschitz, and A. Mai, *Journal of Power Sources*, **182**, 400 (2008).
- E. Konyshova, J. Mertens, H. Penkalla, L. Singheiser, and K. Hilpert, *Journal of The Electrochemical Society*, **154**(12), B1252 (2007).
- J. R. Wilson, W. Kobsiriphat, R. Mendoza, H. Y. Chen, J. M. Hiller, D. J. Miller, K. Thornton, P. W. Voorhees, S. B. Adler, and S. A. Barnett, *Nature Materials*, **5**, 541 (2006).
- J. R. Izzo, Jr., A. S. Joshi, K. N. Grew, W. K. S. Chiu, A. Tkachuk, S. H. Wang, and W. Yun, *Journal of The Electrochemical Society*, **155**(5), B504 (2008).
- J. Vila-Comamala, Y. Pan, J. J. Lombardo, W. M. Harris, W. K. S. Chiu, C. David, and Y. Wang, *Journal of Synchrotron Radiation*, **19**, 705 (2012).
- J. J. Lombardo, R. A. Ristau, W. M. Harris, and W. K. S. Chiu, *Journal of Synchrotron Radiation*, **19**, 789 (2012).
- K. N. Grew, Y. S. Chu, J. Yi, A. A. Peracchio, J. R. Izzo, Jr., Y. Hwu, F. De Carlo, and W. K. S. Chiu, *Journal of The Electrochemical Society*, **157**(6), B783 (2010).
- G. J. Nelson, W. M. Harris, J. R. Izzo, Jr., K. N. Grew, W. K. S. Chiu, Y. S. Chu, J. Yi, J. C. Andrews, Y. Liu, and P. Pianetta, *Applied Physics Letters*, **98**, 173109 (2011).
- A. Hagen, M. L. Traulsen, W. R. Kiebach, and B. S. Johansen, *Journal of Synchrotron Radiation*, **19**, 400 (2012).
- G. J. Nelson, A. Nakajato, B. N. Cassenti, M. B. Degostin, K. R. Bagshaw, A. A. Peracchio, G. Xiao, S. Wang, F. Chen, and W. K. S. Chiu, "A Rapid Analytical Assessment Tool for Three Dimensional Electrode Microstructural Networks with Geometric Sensitivity," in preparation (2013).
- M. Sato, I. Bitter, M. Bender, A. Kaufman, and M. Nakajima, "Teasar: tree-structure extraction algorithm for accurate and robust skeletons", *In Computer Graphics Proceedings. The Eighth Pacific Conference*, 281–449 (2000).
- K. Brinkman and T. Iijima et al., *Japanese Journal of Applied Physics Part 2-Letters & Express Letters*, **46**(4–7), L93 (2007).
- J. Sunarso and S. Baumann et al., *Journal of Membrane Science*, **320**(1–2), 13 (2008).
- H. Takamura and M. Ogawa et al., *Solid State Ionics*, **179**(27–32), 1354 (2008).
- H. X. Luo and H. Q. Jiang et al., *Chemistry of Materials*, **24**(11), 2148 (2012).
- J. Maier, *Physical Chemistry Chemical Physics*, **11**(17), 3011 (2009).
- H. L. Tuller and S. R. Bishop, *Chemistry Letters*, **39**(12), 1226 (2010).
- Y. M. Chiang and E. B. Lavik et al., *Applied Physics Letters*, **69**(2), 185 (1996).
- K. Brinkman and H. L. Tuller et al., *Journal of the Electrochemical Society*, **157**(12), B1852 (2010).
- C. Wagner, *Z. Phys. Chem. B*, **21**, 25 (1933).
- J. A. Lane and J. A. Kilner, *Solid State Ionics*, **136–137**, 997 (2000).
- K. Brinkman and T. Iijima et al., *Mater. Res. Soc. Symp. Proc. Volume 1126*, Warrendale, PA, 2009, **1126**, 145 (2009).
- J. H. Shim and J. S. Park et al., *Acta Materialia*, **60**(1), 1 (2012).
- H. L. Lein, K. Wiik, and T. Grande, *Solid State Ionics*, **177**, 1795 (2006).
- R. Chaim and M. Levin et al., *Advances in Applied Ceramics*, **107**(3), 159 (2008).
- M. Williams and K. Reifsnider, *International Journal of Hydrogen Energy*, **36** (2011).
- F. Kremer and A. Schonhals, Eds., *Broadband Dielectric Spectroscopy*, Springer-Verlag, Berlin (2003).
- E. Barsoukov and J. Ross Macdonald, Eds., *Impedance Spectroscopy: Theory, Experiment and Applications*, Wiley-Interscience (2005).
- K. Reifsnider, Q. Liu, J. M. Adkins, J. Baker, F. Rabbi, and K. Brinkman, *Proc. World Congress on Computational Mechanics*, San Paulo (2012).
- K. Reifsnider, P. Majumdar, and P. Fazzino, *J. Aeronautical Society*, Vol. 113 #1150 (Silver Award, 2010, Royal Aeronautical Society) (2009).
- Q. Liu, *J. Comput. Phys.*, **230**, 8256 (2011).
- Q. Liu, *Int. J. Numer. Meth. Engng.*, **90**, 537 (2012).
- Q. Liu and K. L. Reifsnider, *Comp. Meth. Appl. Mech. Eng.* (under review) (2012).
- J. B. Kim, T. W. Kim, and C. G. Kim, *J. Appl. Poly. Sci.*, **100** (2006).
- J. Liu, C. Duan, W. Yin, W. Mei, R. Smith, and J. Hardy, *Phys. Rev. B*, **70** (2004).
- K. Matsuzaki, N. Shikazono, and N. Kasagi, *Journal of Power Sources*, **196**, 3073 (2011).
- N. Shikazono, D. Kanno, K. Matsuzaki, H. Teshima, S. Sumino, and N. Kasagi, *Journal of the Electrochemical Society*, **157**, B665 (2010).
- C. W. Tanner, K. Fung, and A. V. Virkar, *Journal of the Electrochemical Society*, **144**(1), 21 (1997).
- S. Sunde, *Journal of the Electrochemical Society*, **143**(6), 1930 (1996).
- T. Kenjo, S. Osawa, and K. Fujikawa, *Journal of the Electrochemical Society*, **138**(2), 349 (1991).
- F. Bidrawn, R. Kungas, J. M. Vohs, and R. J. Gorte, *Journal of the Electrochemical Society*, **158**(5), B514 (2011).
- B. N. Cassenti, G. J. Nelson, M. B. Degostin, A. A. Peracchio, and W. K. S. Chiu, "Exact Solutions for Extended Surface Electrochemical Fin Models," in preparation (2013).
- G. J. Nelson, B. N. Cassenti, A. A. Peracchio, and W. K. S. Chiu, *Journal of The Electrochemical Society*, **159**(5), A598 (2012).
- M. H. R. Lankhorst and J. E. ten Elshof, *Journal of Solid State Chemistry*, **130**(2), 302 (1997).
- H. J. M. Bouwmeester, M. W. Den Otter, and B. A. Boukamp, *Journal of Solid State Electrochemistry*, **8**(9), 599 (2004).
- G. J. Nelson, B. N. Cassenti, A. A. Peracchio, and W. K. S. Chiu, "An Analytical Method for Dye-Sensitized Solar Cell Geometric Design," manuscript submitted to *Electrochimica Acta* (2012).
- Q. Liu, X. Dong, G. Xiao, F. Zhao, and F. Chen, *Advanced Materials*, **22**, 5478 (2010).
- G. J. Nelson, W. M. Harris, J. J. Lombardo, J. R. Izzo, W. K. S. Chiu, P. Tanasini, M. Cantoni, J. Van herle, C. Comminellis, J. C. Andrews, Y. Liu, P. Pianetta, and Y. S. Chu, *Electrochemistry Communications*, **13**, 586 (2011).
- C. S. Chen and H. Kruidhof et al., *Solid State Ionics*, **86–8**, 569 (1996).
- C. S. Chen and B. A. Boukamp et al., *Solid State Ionics*, **76**(1–2), 23 (1995).
- B. Wang and M. C. Zhan et al., *Journal of Solid State Electrochemistry*, **10**(8), 625 (2006).
- K. Q. Huang and M. Schroeder et al., *Electrochemical and Solid State Letters*, **2**(8), 375 (1999).
- Q. Liu, *J. Comput. Phys.*, **230**, 8256 (2011).
- Q. Liu, *Int. J. Numer. Meth. Engng.*, **90**, 537 (2012).
- Q. Liu and K. L. Reifsnider, *J. Comput. Phys.*, **235**, 161 (2013).
- G. J. Nelson, A. A. Peracchio, and W. K. S. Chiu, *Journal of Power Sources*, **196**, 4695 (2011).